Euro. Jnl of Applied Mathematics (2009), *vol.* 20, *pp.* 69–91. © 2008 Cambridge University Press
doi:10.1017/S0956792508007651 Printed in the United Kingdom

Crystal precipitation and dissolution in a thin strip

T. L. VAN NOORDEN

Department of Mathematics and Computer Science, Technische Universiteit Eindhoven, P.O. Box 513, 5600 MB Eindhoven, The Netherlands
email: t.l.v.noorden@tue.nl

(*Received 14 November 2007; revised 12 June 2008; first published online 24 July 2008*)

We present a two-dimensional micro-scale model for crystal dissolution and precipitation in a porous medium. The local geometry of the pore is represented as a thin strip and the model allows for changes in the pore volume. A formal limiting argument, for the limit of the width of the strip going to zero, leads to a system of one-dimensional effective upscaled equations. We show that the effective equations allow for travelling-wave solutions and prove the existence and uniqueness of these. Numerical solutions of the effective equations are compared with numerical solutions of the original equations on the thin strip and with analytical results. We also show that a model from the literature that does not allow changes in the pore volume can be obtained from the present model as a formal limit.

1 Introduction

In this paper we derive, using a formal limiting procedure with asymptotic expansions, macroscopic equations for crystal dissolution and precipitation in a porous medium. The microscopic model that serves as the starting point for the limiting process incorporates the change in volume of the pore space as a result of the precipitation–dissolution process. We also study travelling-wave solutions of the macroscopic equations, and the behaviour of solutions of the obtained macroscopic equations is numerically compared to the behaviour of solutions of the corresponding microscopic model.

The dissolution and precipitation of crystals in porous media have been studied also in [7, 12] and [14, 17]. The main difference between the cited papers and the present paper is that in the cited papers it is assumed that the thickness of the layer of crystalline solid attached to the boundary of the flow domain is negligible so that the pore geometry can be assumed to be fixed. In this case the formal homogenization is a standard procedure and the macroscopic equations can be derived straightforwardly.

In this paper we do take into account the change in the pore volume due to the precipitation–dissolution reaction. For the microscale model this results in a free-boundary problem. The free boundary describes the interface between the layer of crystalline solid attached to the pore walls and the fluid occupying the pores. The location of this free boundary is unknown in the model and moves with speed proportional to the local precipitation–dissolution rate. The free boundary forms the main difficulty in performing the formal homogenization for the proposed model, and we show that for the macroscopic

https://doi.org/10.1017/S0956792508007651 Published online by Cambridge University Press

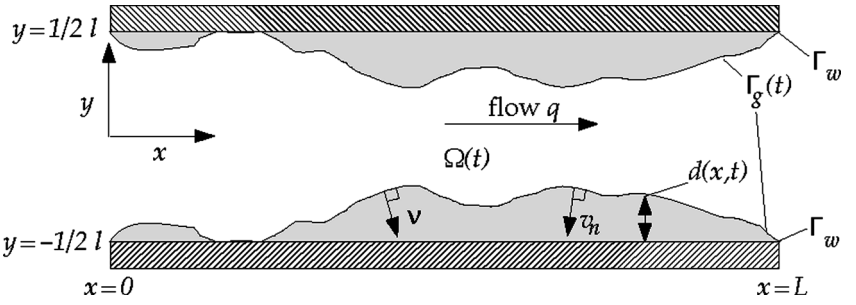


FIGURE 1. Schematic representation of a two-dimensional thin strip with layers of crystalline solid attached to the strip boundary.

model the free boundary gives rise to a permeability and porosity that depend on the local pore geometry. The proposed microscale model with the free boundary has been studied in [16] in a one-dimensional setting and without flow. Other works that study crystal dissolution and precipitation on the microscale are [10] and [9].

Macroscopic equations for reactive transport in porous media, which include the present case of crystal dissolution and precipitation, are of practical importance in many physical, biological and chemical applications. Macroscopic equations for reactive transport in porous media are derived rigorously in e.g. [6]. For the specific case of crystal dissolution and precipitation, macroscopic models are given in [3, 5, 7, 8]. In these papers the presented macroscopic models are analysed, but are not supported by a rigorous derivation. In most of these papers the numerical solution of the proposed model equations is studied, too. Related work, in which the transport of dissolved material is analysed, can be found in [13, 15].

The structure of this paper is as follows. In Section 2 we will discuss the model equations that describe the processes in the thin strip. In Section 3, we will derive, using a formal limiting argument, the effective equations for the limit of the thickness of the strip to zero. Travelling-wave solutions of the effective equations are studied in Section 4. In Section 5 we show that we obtain the effective equations studied in [7, 12] for the fixed geometry model as formal limit of the variable geometry model if the density of the crystalline solid goes to infinity. We also compare analytical results obtained for the travelling-wave solutions to the results for the effective equations studied in [7, 12]. In Section 6 we present and compare numerical results for both the microscale model and the effective equations. The microscale model, containing the free boundary, is discretized using the Arbitrary Lagrangian–Eulerian method.

2 Model equations

We consider the following model for crystal dissolution and precipitation in a pore. The pore space is represented by a two-dimensional thin strip of length L (m) and width l (m) (for a schematic figure, see Figure 1). The two-dimensional bounded domain Υ, representing the strip, is given by

$$\Upsilon := \{(x, y) \in \mathbb{R}^2 \mid 0 \leqslant x \leqslant L,\ -l/2 \leqslant y \leqslant l/2\},$$

https://doi.org/10.1017/S0956792508007651 Published online by Cambridge University Press

A layer of crystalline solid may be attached to the boundaries of the strip, and we assume that the thickness of the layers on both the upper and the lower boundaries are equal, so that the geometry is symmetric with respect to the x-axis. The thickness of this layer is given by $d(x,t)$ (m). Let

$$\Omega(t) := \{(x,y)\,|\,0 \leqslant x \leqslant L,\ -(l/2 - d(x,t)) \leqslant y \leqslant (l/2 - d(x,t))\}$$

denote the (variable) region occupied by a fluid in which cations and anions are dissolved. Here we assume that $d(x,t) < l/2$. When $d = l/2$ the strip is blocked by the crystalline solid and we do not consider this situation in the present paper.

The boundary of $\Omega(t)$ can be split into three parts: the interface of the crystalline layer with the fluid, denoted by $\Gamma_g(t)$, which is defined by

$$\Gamma_g(t) := \{(x,y)\,|\,0 < x < L,\ y = \pm(l/2 - d(x,t))\},$$

the boundary at $x = 0$, denoted by $\Gamma_i(t)$,

$$\Gamma_i(t) := \{(x,y)\,|\,x = 0,\ -(l/2 - d(0,t)) \leqslant y \leqslant l/2 - d(0,t)\}$$

and the boundary at $x = L$, denoted by $\Gamma_o(t)$,

$$\Gamma_o(t) := \{(x,y)\,|\,x = L,\ -(l/2 - d(L,t)) \leqslant y \leqslant l/2 - d(L,t)\}.$$

In a precipitation reaction n_1 cations and n_2 anions can precipitate in the form of one molecule of a crystalline solid, which is attached to the boundary. The reverse dissolution reaction is also possible. Let c_1 and c_2 (mol/m^2) denote the molar concentration of the cations and anions, respectively. Then c_i, for $i = 1,2$, satisfies the convection–diffusion equation in $\Omega(t)$

$$\partial_t c_i = \nabla \cdot (D_i \nabla c_i - q c_i), \quad \text{for } i = 1,2,$$

where D_i, for $i = 1,2$, is the diffusion coefficient and q (m/s) denotes the fluid velocity.

At this point we make the simplifying, but restrictive, assumption that the diffusion coefficients are equal (see also [14]):

$$D := D_1 = D_2.$$

Furthermore we assume that in the fluid phase the sum of the molar concentrations of the cations, the anions and the solvent is constant, which may be justified by assuming that the concentration of ions in the fluid is small. We denote the constant molar concentration of the fluid phase by ρ_f (mol/m^2).

At the interface of the layer attached to the boundary of the strip, we have by conservation of mass of the anions and cations the following *Rankine–Hugoniot condition* [4]

$$v \cdot (D \nabla c_i - q c_i) = v_n (n_i \rho_c - c_i), \text{ on } \Gamma_g(t), \ \ i = 1,2, \tag{2.1}$$

where ρ_c (mol/m^2) is the molar density of the crystalline solid and v is the outward pointing unit normal given by

$$v = (\partial_x d, -1)^T / \sqrt{1 + (\partial_x d)^2} \tag{2.2}$$

https://doi.org/10.1017/S0956792508007651 Published online by Cambridge University Press

for the lower boundary and v_n (m/s) is the outward normal velocity of the interface. Similarly, by conservation of the total mass, we have the Rankine–Hugoniot condition

$$v \cdot (-q\rho_f) = v_n((n_1+n_2)\rho_c - \rho_f), \text{ on } \Gamma_g(t). \tag{2.3}$$

The normal velocity of the interface is proportional to the local difference between the dissolution and precipitation rates and is given by (see e.g. [7])

$$\rho_c v_n(c_1,c_2,x) = -(k_p r(c_1,c_2) - k_d w(x)), \quad \text{for } x \in \Gamma_g(t), \tag{2.4}$$

where k_p and k_d are positive rate constants (mol/m s) and $r(c_1,c_2)$ is a rate function describing the precipitation rate. A typical example is given by the law of mass action kinetics, leading to

$$r(c_1,c_2) = k_m c_1^{n_1} c_2^{n_2}, \tag{2.5}$$

with k_m $((\text{mol/m}^2)^{-(n_1+n_2)})$ as a constant. The dissolution rate $w(x)$ is set-valued and is given by

$$w(x) \in H(d(x,t)),$$

where H is the set-valued Heaviside graph,

$$H(u) = \begin{cases} \{0\}, & \text{if } u < 0, \\ [0,1], & \text{if } u = 0, \\ \{1\}, & \text{if } u > 0. \end{cases}$$

This description of the dissolution rate follows from the generally accepted assumption [7] that the activity of the crystalline solid is a positive constant. For a more extensive derivation and discussion of the dissolution and precipitation rates, we refer to [7, 16] and the references therein.

The velocity of a point $s(t)$ that moves on the lower part of the boundary $\Gamma_g(t)$, with coordinates $s(t) = (x(t), -\frac{1}{2}l + d(x(t),t))$, is given by

$$s'(t) = \big(x'(t), \partial_x d(x(t),t)x'(t) + \partial_t d(x(t),t)\big).$$

The normal velocity v_n of the boundary at $s(t)$, which is the normal component of $s'(t)$, is obtained by taking the inner product with the unit normal:

$$v_n = v \cdot s'(t) = -\partial_t d / \sqrt{1 + (\partial_x d)^2}. \tag{2.6}$$

Combining (2.2), (2.4) and (2.6), we obtain the following relation for d:

$$\rho_c \partial_t d \in (k_p r(c_1,c_2) - k_d H(d))\sqrt{1 + (\partial_x d)^2}. \tag{2.7}$$

At the parts of the boundary $\Gamma_i(t)$ and $\Gamma_o(t)$, we impose

$$\begin{cases} c_1 = c_{b1} \text{ and } c_2 = c_{b2} & \text{on } \Gamma_i(t), \\ \partial_x c_1 = \partial_x c_2 = 0 & \text{on } \Gamma_o(t), \end{cases}$$

where c_{b1} and c_{b2} are given non-negative constants.

https://doi.org/10.1017/S0956792508007651 Published online by Cambridge University Press

Now we turn to the equations that describe the fluid flow and to the boundary conditions that couple the flow with the dissolution–precipitation process. The fluid flow is assumed to be described by the Stokes equations

$$\mu \Delta q = \nabla p,$$
$$\nabla \cdot q = 0,$$

for the fluid velocity q (m/s) and pressure p (kg/m s^2), where μ (kg/m s) is the viscosity. In order to derive a boundary condition for q, we consider the boundary condition (2.3), obtained by the conservation of the total mass. Assuming no slip along the boundary, so that the flow is perpendicular to the boundary, gives

$$q = K v_n \nu, \text{ on } \Gamma_g(t), \quad \text{with } K = \frac{\rho_f - (n_1 + n_2)\rho_c}{\rho_f}. \tag{2.8}$$

The boundary condition for q at the parts of the boundary $\Gamma_i(t)$ and $\Gamma_o(t)$ has to be such that it is consistent with $\nabla \cdot q = 0$. Therefore we impose $q = q_b$ on $\Gamma_i(t)$ and $\Gamma_o(t)$, where q_b is given such that

$$\int_{\Gamma_i(t) \cup \Gamma_o(t)} \nu \cdot q_b = - \int_{\Gamma_g(t)} K v_n.$$

2.1 Dimensionless form

We make the simplifying assumptions

$$n_1 = n_2, \quad c_1(x, y, 0) = c_2(x, y, 0) \quad \text{and} \quad c_{b1} = c_{b2}.$$

By the uniqueness of solutions of parabolic equations on non-cylindrical domains, under appropriate assumptions on the regularity of the free boundary [1] (see also [16] for existence and uniqueness results in a one-dimensional setting), these assumptions imply that $c_1(x, y, t) = c_2(x, y, t) = c(x, y, t)$. We introduce reference values t_{ref}, $x_{\text{ref}} := L$ and $y_{\text{ref}} := L$ for the time and space variables t, x and y. We also introduce a reference value for the concentration c, denoted by c_{ref}, a reference value q_{ref} for the fluid velocity, given by $q_{\text{ref}} := L/t_{\text{ref}}$, and a reference value for the pressure denoted by p_{ref}. Since we are interested in the limit as the thickness of the strip tends to zero, we introduce the dimensionless aspect ratio $\epsilon := l/L$ as a small parameter. Furthermore we define the dimensionless quantities

$$t := t/t_{\text{ref}}, \quad x := x/x_{\text{ref}}, \quad y := y/y_{\text{ref}}, \quad u^\epsilon := c/c_{\text{ref}}, \quad d^\epsilon := d/l,$$
$$q^\epsilon := q/q_{\text{ref}}, \quad p^\epsilon := p/p_{\text{ref}}, \quad \rho_f := \rho_f/c_{\text{ref}}, \quad \rho := \frac{n_1 \rho_c}{c_{\text{ref}}},$$
$$r(u) := \frac{k_p}{k_d} r(c_{\text{ref}} u, c_{\text{ref}} u), \quad k := \frac{k_d t_{\text{ref}} n_1}{c_{\text{ref}} l}, \quad D := \frac{D t_{\text{ref}}}{L^2}, \quad \mu := \frac{\mu L q_{\text{ref}}}{l^2 p_{\text{ref}}},$$

https://doi.org/10.1017/S0956792508007651 Published online by Cambridge University Press

where we use the superscripts for u^ϵ, d^ϵ, q^ϵ and p^ϵ to stress the dependence on the small parameter ϵ, and obtain the equations

$$\begin{cases} \partial_t u^\epsilon = \nabla \cdot (D\nabla u^\epsilon - q^\epsilon u^\epsilon), \\ \epsilon^2 \mu \Delta q^\epsilon = \nabla p^\epsilon, \\ \nabla \cdot q^\epsilon = 0, \\ u^\epsilon,\ q^\epsilon \text{ and } p^\epsilon \text{ symmetric around } y = 0, \end{cases} \quad \text{in } \Omega^\epsilon(t) \tag{2.9}$$

$$\begin{cases} \rho \partial_t d^\epsilon = k(r(u^\epsilon) - w)\sqrt{1 + (\epsilon \partial_x d^\epsilon)^2}, \\ w \in H(d^\epsilon), \\ \rho v^\epsilon \cdot (D\nabla u^\epsilon - q^\epsilon u^\epsilon) = -\epsilon k(r(u^\epsilon) - w)(\rho - u^\epsilon), \\ \rho q^\epsilon = -\epsilon K k(r(u^\epsilon) - w) v^\epsilon, \end{cases} \quad \text{on } \Gamma^\epsilon(t) \tag{2.10}$$

$$\begin{cases} u^\epsilon = u_b, \quad q^\epsilon = q_{bi} & \text{on } \Gamma_i^\epsilon(t) \\ u_x^\epsilon = 0, \quad q^\epsilon = q_{bo} & \text{on } \Gamma_o^\epsilon(t) \end{cases} \tag{2.11}$$

$$\begin{cases} u^\epsilon(x, y, 0) = u_I(x, y), \\ \rho d^\epsilon(x, 0) = v_I(x), \end{cases} \tag{2.12}$$

where

$$\begin{aligned} \Omega^\epsilon(t) &:= \{(x, y) \,|\, 0 \leqslant x \leqslant 1,\ -\epsilon(1/2 - d^\epsilon(x, t)) \leqslant y \leqslant \epsilon(1/2 - d^\epsilon(x, t))\}, \\ \Gamma^\epsilon(t) &:= \{(x, y) \,|\, 0 \leqslant x \leqslant 1,\ y = \pm\epsilon(1/2 - d^\epsilon(x, t))\}, \\ \Gamma_i^\epsilon(t) &:= \{(x, y) \,|\, x = 0,\ -\epsilon(l/2 - d^\epsilon(0, t)) \leqslant y \leqslant \epsilon(l/2 - d^\epsilon(0, t))\}, \\ \Gamma_o^\epsilon(t) &:= \{(x, y) \,|\, x = 1,\ -\epsilon(l/2 - d^\epsilon(1, t)) \leqslant y \leqslant \epsilon(l/2 - d^\epsilon(1, t))\}, \end{aligned}$$

and where v^ϵ is the outward pointing normal to $\Gamma^\epsilon(t)$, which on the lower part of the boundary is given by

$$v^\epsilon = (\epsilon \partial_x d^\epsilon, -1)^T / \sqrt{1 + (\epsilon \partial_x d^\epsilon)^2}. \tag{2.13}$$

By the scaling, the restriction that $d < l/2$ now becomes $d^\epsilon < 1/2$. The initial concentration of the dissolved material is given by $u_I(x, y)$ and the function $v_I(x)$ is an initial surface concentration of the crystalline solid.

The dimensionless number k is usually referred to as the Damköhler number and expresses the ratio between the diffusion and the reaction time scale. The auxiliary function w acts as the scaled dissolution rate. When $d^\epsilon > 0$, $w = 1$ and when $d^\epsilon = 0$, we have $w \leqslant r(u^\epsilon)$. With respect to the reaction rate function $r(u)$, we assume

(1) $r : \mathbb{R} \to [0, \infty)$ is locally Lipschitz;

(2) a unique $\tilde{u} \in [0, \rho)$ exists such that $r(u) = 0$ for all $u \leqslant \tilde{u}$ and $r(u)$ is strictly increasing if $u > \tilde{u}$;

(3) a unique $u_s \in (\tilde{u}, \rho)$ exists such that $r(u_s) = 1$.

Note that these assumptions are fulfilled in the typical case of the law of mass action kinetics (2.5).

https://doi.org/10.1017/S0956792508007651 Published online by Cambridge University Press

Since we assumed that the molar concentration of the fluid phase is constant, it makes sense to assume also that $2u_s < \rho_f$. Using this assumption, and the expression for K in (2.8), we obtain the following bounds for K, which we will use later on

$$\frac{u_s - \rho}{u_s} < K < 1. \tag{2.14}$$

Furthermore, we assume the following inequalities for the initial concentrations

$$0 \leqslant u_I < \min(\rho, \rho_f/2),$$
$$0 \leqslant \rho v_I < 1/2.$$

3 Thin strip

In this section we derive using a formal limiting argument the effective equations in a strip with vanishing width. We assume the following asymptotic expansions for u^ϵ, d^ϵ, q^ϵ and p^ϵ in the small parameter ϵ

$$u^\epsilon(x,y,t) = u_0(x, \frac{y}{\epsilon}, t) + \epsilon u_1(x, \frac{y}{\epsilon}, t) + \epsilon^2(...), \tag{3.1}$$
$$d^\epsilon(x,t) = d_0(x,t) + \epsilon d_1(x,t) + \epsilon^2(...), \tag{3.2}$$
$$q^\epsilon(x,y,t) = q_0(x, \frac{y}{\epsilon}, t) + \epsilon q_1(x, \frac{y}{\epsilon}, t) + \epsilon^2(...), \tag{3.3}$$
$$p^\epsilon(x,y,t) = p_0(x, \frac{y}{\epsilon}, t) + \epsilon p_1(x, \frac{y}{\epsilon}, t) + \epsilon^2(...), \tag{3.4}$$

where it should be noted that the $q_i(x,z,t)$ are vectors, with $q_i = (q_i^{(1)}, q_i^{(2)})$, for $i = 0, 1, 2, ...$ Also note that the second vertical-coordinate of the variables $u_i(x,z,t)$, $q_i(x,z,t)$ and $p_i(x,z,t)$ is rescaled so that it is defined on the domain

$$\tilde{\Omega}(t) := \{(x,z) \,|\, 0 \leqslant x \leqslant 1,\ -1/2 + d^\epsilon \leqslant z \leqslant 1/2 - d^\epsilon\}.$$

If we substitute the expansion for u^ϵ in the convection–diffusion equation, we obtain

$$\begin{aligned}\partial_t u_0 = {} & \partial_x\big(D\partial_x u_0 - q_0^{(1)} u_0\big) + \epsilon^{-1}\partial_z\big(\epsilon^{-1} D\partial_z u_0 - q_0^{(2)} u_0\big) + \epsilon^{-1}\partial_z(D\partial_z u_1) \\ & + \partial_y(D\partial_y u_2) - \partial_z\big(q_1^{(2)} u_0 + q_0^{(2)} u_1\big) + \epsilon(\ldots).\end{aligned}$$

For the boundary condition we obtain, using (2.10_1) and (2.10_3),

$$\begin{aligned}\epsilon\partial_x d_0\big(D\partial_x u_0 - q_0^{(1)} u_0\big) - \big(\epsilon^{-1} D\partial_y u_0 - q_0^{(2)} u_0\big) + D\partial_y u_1 + \epsilon D\partial_y u_2 \\ + \epsilon\big(q_1^{(2)} u_0 + q_0^{(2)} u_1\big) = -\epsilon\partial_t d_0(\rho - u_0) + \epsilon^2(...)\end{aligned}$$

at $z = -(1/2 - d^\epsilon)$. Combining the lowest order terms of both equations gives the following set of equations

$$\begin{cases} \partial_{zz} u_0 = 0, & \text{in } \tilde{\Omega}(t) \\ \partial_z u_0 = 0, & \text{at } z = -1/2 + d^\epsilon \text{ and } z = 1/2 - d^\epsilon. \end{cases}$$

From these equations we conclude that u_0 does not depend on z.

https://doi.org/10.1017/S0956792508007651 Published online by Cambridge University Press

Now we proceed to integrate the convection–diffusion equation for u^ϵ. Note that we integrate over the coordinate y, not over the rescaled coordinate z:

$$\frac{1}{\epsilon}\int_{-\epsilon(1/2-d^\epsilon)}^{\epsilon(1/2-d^\epsilon)} \partial_t u^\epsilon \, dy = \frac{1}{\epsilon}\int_{-\epsilon(1/2-d^\epsilon)}^{\epsilon(1/2-d^\epsilon)} \partial_x\big(D\partial_x u^\epsilon - q^{\epsilon(1)}u^\epsilon\big) + \partial_y\big(D\partial_y u^\epsilon - q^{\epsilon(2)}u^\epsilon\big)\, dy.$$

Interchanging differentiation and integrals results in

$$\begin{aligned}\partial_t\left(\frac{1}{\epsilon}\int_{-\epsilon(1/2-d^\epsilon)}^{\epsilon(1/2-d^\epsilon)} u^\epsilon \, dy\right) + 2\partial_t d^\epsilon u^\epsilon|_{y=-\epsilon(1/2-d^\epsilon)} &= \partial_x\left(\frac{1}{\epsilon}\int_{-\epsilon(1/2-d^\epsilon)}^{\epsilon(1/2-d^\epsilon)} \big(D\partial_x u^\epsilon - q^{\epsilon(1)}u^\epsilon\big)\, dy\right)\\ &+ 2\partial_x d^\epsilon\big(D\partial_x u^\epsilon - q^{\epsilon(1)}u^\epsilon\big)|_{y=-\epsilon(1/2-d^\epsilon)} - \frac{2}{\epsilon}\big(D\partial_y u^\epsilon - q^{\epsilon(2)}u^\epsilon\big)|_{y=-\epsilon(1/2-d^\epsilon)}.\end{aligned}$$

Using the boundary condition (2.10_3), we obtain

$$\begin{aligned}&\partial_t\left(\frac{1}{\epsilon}\int_{-\epsilon(1/2-d^\epsilon)}^{\epsilon(1/2-d^\epsilon)} u^\epsilon \, dy\right) + 2\partial_t d^\epsilon u^\epsilon|_{y=-\epsilon(1/2-d^\epsilon)}\\ &\quad= \partial_x\left(\frac{1}{\epsilon}\int_{-\epsilon(1/2-d^\epsilon)}^{\epsilon(1/2-d^\epsilon)} \big(D\partial_x u^\epsilon - q^{\epsilon(1)}u^\epsilon\big)\, dy\right) - 2\partial_t d^\epsilon(\rho - u^\epsilon)|_{y=-\epsilon(1/2-d^\epsilon)}. \qquad (3.5)\end{aligned}$$

Now we substitute the expansions (3.1), (3.2) and (3.3) in equation (3.5), and change the variable of integration from y to z. Retaining only the terms independent of ϵ gives

$$\begin{aligned}&\partial_t\left(\int_{-(1/2-d_0)}^{(1/2-d_0)} u_0(x,z,t)\, dz\right) + 2\partial_t d_0(x,t)u_0(x,z,t)|_{z=-(1/2-d_0(x,t))}\\ &\quad= \partial_x\left(\int_{-(1/2-d_0)}^{(1/2-d_0)} (D\partial_x u_0(x,z,t) - q_0^{(1)}(x,z,t)u_0(x,z,t))\, dz\right)\\ &\qquad - 2\partial_t d_0(x,t)(\rho - u_0(x,z,t))|_{z=(1/2-d_0(x,t))}.\end{aligned}$$

We use the fact that u_0 does not depend on z, i.e. $u_0(x,z,t) = u_0(x,t)$, and obtain

$$\partial_t((1-2d_0)u_0 + 2\rho d_0) = \partial_x(D(1-2d_0)\partial_x u_0 - \bar{q}u_0), \qquad (3.6)$$

where $\bar{q}$ denotes the averaged velocity

$$\bar{q} = \int_{-1/2+d_0}^{1/2-d^0} q_0^{(1)}\, dz.$$

Now we turn our attention to the flow problem. We integrate both sides of the equation $\nabla\cdot q^\epsilon = 0$ over a portion of the strip of length δx, denoted by

$$Y = \{(v,w)\,|\,x_1 \leqslant v \leqslant x_1 + \delta x, |w| \leqslant \epsilon(1/2-d)\}.$$

https://doi.org/10.1017/S0956792508007651 Published online by Cambridge University Press

We compute

$$0 = \int_Y \nabla \cdot q^\epsilon \, dV = \int_{-\epsilon(1/2-d)}^{\epsilon(1/2-d)} q^{\epsilon(1)}|_{x=x_1+\delta x} \, dy - \int_{-\epsilon(1/2-d)}^{\epsilon(1/2-d)} q^{\epsilon(1)}|_{x=x_1} \, dy + 2\int_{x_1}^{x_1+\delta x} v \cdot q^\epsilon|_{y=\epsilon(1/2-d)} \sqrt{1+(\epsilon d_x)^2} \, dx.$$

Dividing by δx, taking the limit $\delta x \to 0$ and collecting the lowest order terms in ϵ gives

$$\partial_x \bar{q} - 2K \partial_t d_0 = 0. \tag{3.7}$$

Substituting the expansions for q^ϵ and p^ϵ in (2.9$_{2,3}$) and collecting the terms with the lowest order in ϵ yields the set of equations

$$\begin{cases} \partial_z p_0 = 0, \\ \mu \partial_{zz} q_0^{(1)} = \partial_x p_0, \qquad \text{in } \tilde{\Omega}(t), \\ \partial_z q_0^{(2)} = 0, \end{cases}$$

$$q_0^{(1)} = q_0^{(2)} = 0 \quad \text{for} \quad z = -1/2 + d_0 \quad \text{and} \quad z = 1/2 - d_0.$$

We conclude that p_0 does not depend on the z-coordinate, and that $q_0^{(2)} \equiv 0$. Furthermore, we can solve for $q_0^{(1)}$ in terms of $\partial_x p_0$:

$$q_0^{(1)}(x,z,t) = (z^2 - (1/2 - d^0(x,t))^2) \frac{\partial_x p_0(x,t)}{2\mu}.$$

Integrating this equation along the z-coordinate yields

$$\bar{q} = \frac{\partial_x p_0}{2\mu} \int_{-1/2+d_0}^{1/2-d_0} (z^2 - (1/2-d^0)^2) \, dz = -\frac{2\partial_x p_0}{3\mu} (1/2 - d_0)^3,$$

so that we can now write an expression for the pressure gradient

$$\partial_x p_0 = -\frac{3\mu \bar{q}}{2(1/2-d_0)^3}. \tag{3.8}$$

In order to derive an effective equation for d_0, we first regularize the set-valued Heaviside graph, so that we obtain

$$\partial_t d^\epsilon = k(r(u^\epsilon) - H_\delta(d^\epsilon)) \sqrt{1 + (\epsilon \partial_x d^\epsilon)^2},$$

where, for $\delta > 0$,

$$H_\delta(d) := \begin{cases} 0, & \text{if } d < 0, \\ d/\delta, & \text{if } d \in [0, \delta], \\ 1, & \text{if } d > \delta. \end{cases}$$

Since r and H_δ are both Lipschitz, we obtain, after substituting the asymptotic expansions (3.1)–(3.2),

$$\rho \partial_t d_0 = k(r(u_0) - H_\delta(d_0)) + \epsilon(...).$$

https://doi.org/10.1017/S0956792508007651 Published online by Cambridge University Press

Only keeping terms independent of ϵ, and letting $\delta \to 0$, we obtain (see e.g. [14, Theorem 2.21])

$$\rho \partial_t d_0 \in k(r(u_0) - H(d_0)). \tag{3.9}$$

Collecting the equations (3.6), (3.7) and (3.9), we arrive at the following system of equations, for the unknowns $u_0(x,t)$, $\bar{q}(x,t)$ and $d_0(x,t)$,

$$\begin{cases} \partial_t((1-2d_0)u_0 + 2\rho d_0) = \partial_x(D(1-2d_0)\partial_x u_0 - \bar{q}u_0), \\ \partial_x \bar{q} - 2K\partial_t d_0 = 0, \\ \rho \partial_t d_0 \in k(r(u_0) - H(d_0)). \end{cases} \tag{3.10}$$

4 Travelling waves

In this section we will study travelling-wave solutions of the system (3.10), which we derived taking into account the thickness of the crystalline layer. We will prove the existence and uniqueness of travelling-wave solutions, and in the proofs we will follow closely parts of Sections 1, 2 and 3 of [12], where such solutions are studied for a model that is derived assuming that the thickness of the crystalline layer attached to the boundary of the strip is negligible. In Section 5 we will discuss in more detail the relation between these two situations.

For notational convenience we drop the subscripts and bars from the unknowns, and we study the following system of equations for the unknown functions $u(x,t)$, $d(x,t)$ and $q(x,t)$:

$$\begin{cases} \partial_t((1-2d)u + 2\rho d) - \partial_x((1-2d)D\nabla u - qu) = 0, \\ \rho \partial_t d \in k(r(u) - H(d)), \\ \partial_x q - 2K\partial_t d = 0. \end{cases} \tag{4.1}$$

We look for non-negative travelling-wave solutions, i.e. $u = u(\eta)$, $d = d(\eta)$ and $q = q(\eta)$ with $\eta = x - at$, and $d < 1/2$, satisfying

$$\left.\begin{array}{l} -a((1-2d)u + 2\rho d)' - ((1-2d)Du' - qu)' = 0, \\ -a\rho d' \in k(r(u) - H(d)), \\ q' + 2aKd' = 0, \end{array}\right\} \quad \text{in } \mathbb{R}$$

and boundary conditions

$$\begin{aligned} &u(-\infty) = u^*, \ u(\infty) = u_*, \\ &d(-\infty) = d^*, \ d(\infty) = d_*, \\ &q(-\infty) = q^*, \end{aligned} \tag{4.2}$$

where we assume that $0 \leqslant u^*, u_*, q^*$ and $0 \leqslant d^*, d_* < 1/2$. To define the notion of solutions of the travelling-wave equations we introduce

$$w := \frac{1}{k}(a\rho d' + kr(u)) \in H(d),$$

as a new variable.

https://doi.org/10.1017/S0956792508007651 Published online by Cambridge University Press

Definition 1 The set (u, d, w, q, a), with u, d, w and q being functions defined on $\mathbb{R}$ and a a real number, is called a travelling wave if

(i) $u \in C^1(\mathbb{R})$, $d \in C^1_{pw}(\mathbb{R})$, $w \in C_{pw}(\mathbb{R})$, $q \in C^1_{pw}(\mathbb{R})$,

(ii) u, $w \geqslant 0$ and $0 \leqslant d < 1/2$

(iii) $q' + 2aKd' = 0$,

(iv) $0 \leqslant w \leqslant 1$, $w = 1$ on $\{d > 0\}$,

(v) $((1-2d)Du' + 2a\rho d)' = (qu - a(1-2d)u)'$,

(vii) $-a\rho d' + kw = kr(u)$,

(viii) u, d and q satisfy the boundary conditions (4.2).

We use $C_{pw}(\mathbb{R})$ to denote the piecewise continuous functions on $\mathbb{R}$ (with finitely many points of discontinuity), which are continuous from the right and $C^1_{pw}(\mathbb{R})$ to denote those $u \in C(\mathbb{R})$ for which $f \in C_{pw}(\mathbb{R})$ exists such that $u' = f$ except at the points of discontinuity of f.

Integrating equation (iii) in Definition 1, we obtain

$$q = q^* + 2aK(d^* - d). \tag{4.3}$$

For $\eta \to \infty$, we obtain

$$q_* := q(+\infty) = q^* + 2aK\delta d,$$

where $\delta d := d^* - d_*$. Integration of the equation in Definition 4.1(v) leads to

$$(1-2d)Du' + 2a\rho d = qu - a(1-2d)u + A \tag{4.4}$$

for some $A \in \mathbb{R}$. For $\eta \to \pm\infty$ this equation leads to a set of equations for a and A, which results in

$$a = \frac{\delta u}{(2\rho + 2Ku_*)\delta d + \delta((1-2d)u)} q^*, \tag{4.5}$$

$$A = a(2\rho d^* + (1-2d^*)u^*) - q^* u^*, \tag{4.6}$$

where $\delta u := u^* - u_*$, $\delta d := d^* - d_*$ and $\delta((1-2d)u) := (1-2d^*)u^* - (1-2d_*)u_*$. Substituting (4.6) in (4.4) gives the following equation for u:

$$(1-2d)Du' = (q^* - a)(u - u^*) - 2a(\rho + Ku)(d - d^*) + 2a(du - d^*u^*). \tag{4.7}$$

For a travelling wave to exist, we need that the boundary conditions on u and d are equilibrium points for the differential equations. Considering the u-equation this is guaranteed by the expression for the wave speed. For the d-equation, it requires the additional conditions

$$\begin{aligned} r(u^*) &\in H(d^*), \\ r(u_*) &\in H(d_*). \end{aligned} \tag{4.8}$$

https://doi.org/10.1017/S0956792508007651 Published online by Cambridge University Press

We first investigate the possible combinations of boundary conditions for which travelling waves can exist:

- $d_*, d^* > 0$ and $d_* \neq d^*$: then it follows from (4.8) that $u^* = u_* = u_s$. By (2.14), the denominator in (4.5) is not equal to zero, and we have $a = 0$. In this case (4.7) implies that $u = u_s$ on $\mathbb{R}$. This solution describes the situation of an abitrary, stationary crystal distribution in the presence of saturated fluid.
- $d_* = d^* = 0$ and $u^* \neq u_*$: in this case $a = q^*$ and (4.7) reduces to

$$(1 - 2d)u' = -2q^* d(\rho - u).$$

Now we need to consider two cases: (a) $d = 0$ on $\mathbb{R}$. This implies, by the equation above, that u is constant, which is in contradiction with the conditions $u(-\infty) = u^*$ and $u(\infty) = u_*$, with $u^* \neq u_*$. (b) $d(\eta_0) > 0$ and $d'(\eta_0) = 0$ for some η_0. This implies $u(\eta_0) = u_s$ and $u(\eta) > u_s$ for $\eta < \eta_0$. This means that $u^* > u_s$, which is in contradiction with the boundary condition (4.8_1).

Thus to obtain a non-trivial solution we need that precisely one of the boundary conditions on d is zero. We are left with the following two classes:

$$\text{I} \begin{cases} d_* > 0, & d^* = 0, \\ u_* = u_s, & 0 \leqslant u^* < u_s, \end{cases}$$

$$\text{II} \begin{cases} d^* > 0, & d_* = 0, \\ u^* = u_s, & 0 \leqslant u_* < u_s. \end{cases}$$

It can easily be checked, using the bounds (2.14), that for both classes $q^* > a > 0$. Here, class I represents a wave of precipitation and class II a wave of dissolution.

We do not consider the cases

$$d^* = d_* > 0, \quad u^* = u_* = u_s, \quad \text{and}$$
$$d^* = d_* = 0, \quad u^* = u_* \leqslant u_s.$$

In these cases the wave speed a is not uniquely determined: the trivial constant solutions exist for arbitrary a. Just as in [12] we do not think that there exist non-trivial solutions in these cases, but we cannot exclude these at the moment.

We state the following proposition without proof, as the proof runs exactly along the lines of the proof of Proposition 2.1 in [12].

Proposition 4.2 *Let (u, d, w, q, a) be a travelling wave with boundary conditions from class I or class II. Then*

(i) $u < u_s$ *on* $\mathbb{R}$,

(ii) d *is continuously differentiable and* $d' > 0$ *in* $\{d > 0\}$.

The second statement in Proposition 4.2 immediately gives:

https://doi.org/10.1017/S0956792508007651 Published online by Cambridge University Press

Corollary 4.3 *No travelling wave exists with boundary conditions from class II.*

The following proposition is part (i) of Proposition 2.3 in [12], to which paper we refer to for the proof.

Proposition 4.4 *There exists an* $L \in \mathbb{R}$ *such that*

$$d(\eta) = \begin{cases} 0, & \text{for } -\infty < \eta \leqslant L, \\ > 0, & \text{for } \eta > L. \end{cases}$$

Now we are in a position to prove the following existence result.

Theorem 4.5 *For any set of boundary conditions from class I, there exists a travelling wave.*

Proof We set the L from Proposition 4.4 by translation to $L = 0$, which means that the solution has to satisfy

$$\begin{aligned} d(\eta) &> 0, \quad \text{for} \quad \eta > 0, \\ d(\eta) &= 0, \quad \text{for} \quad \eta \leqslant 0, \\ w(\eta) &= 1, \quad \text{for} \quad \eta > 0. \end{aligned}$$

The travelling-wave functions u, d and w are found by matching the solutions of the following initial value problems:

$$(P^+) \begin{cases} u' = \dfrac{(q^* - a)(u - u^*) - 2ad(\rho - (1 - K)u)}{(1 - 2d)D} =: f_1(u, d), & \text{for } \eta > 0, \\ d' = \dfrac{k}{a\rho}(1 - r(u)) =: f_2(u, d), & \text{for } \eta > 0, \\ u(0) = u_0 \in (u^*, u_s), \ \text{and} \ d(0) = 0. \end{cases}$$

$$(P_-) \begin{cases} u' = \dfrac{q^* - a}{D}(u - u^*), & \text{for } \eta < 0, \\ w = r(u), & \text{for } \eta < 0, \\ u(0) = u_0. \end{cases}$$

We will now use a shooting argument in the u, d phase plane. First we will proof the existence of an initial value u_0 for Problem (P^+) such that

$$(u(\eta), d(\eta)) \to (u_s, d_*) \ \text{as} \ \eta \to \infty.$$

Subsequently we solve for this value of u_0 Problem (P^-).

We investigate the sign of the functions f_1 and f_2. We have for $u \in [u^*, u_s]$, $d \in [0, d_*]$:

$$\begin{aligned} f_1(u, d) > 0 \,(\text{resp. } < 0) \Leftrightarrow f(u) := \frac{(q^* - a)(u - u^*)}{2a(\rho - (1 - K)u)} < d \,(\text{resp. } > d), \\ f_2(u, d) > 0 \Leftrightarrow u < u_s. \end{aligned}$$

https://doi.org/10.1017/S0956792508007651 Published online by Cambridge University Press

It is clear that $f(u)$ is increasing for $u > 0$. Furthermore, we have $f(u^*) = 0$, and, by the expression (4.5) for a, we have $f(u_s) = d_*$.

For the set $S := \{(u,d) \mid u^* < u < u_s,\ d_* < d < f(u)\}$ we consider the following parts of its boundary

$$\partial S_1 := \{(u,d) \mid u^* < u < u_s,\ d = f(u)\},$$
$$\partial S_2 := \{(u,d) \mid u = u_s,\ 0 < d < d_*\}.$$

In the interval (u^*, u_s) we distinguish the subsets A and B according to the following criteria. We say that $\alpha \in A$ if the positive half-orbit corresponding to the solution of Problem (P^+) with $u(0) = \alpha$, $d(0) = 0$ leaves the set S through the boundary ∂S_1. Similarly, $\beta \in B$ if the positive half-orbit starting from $u(0) = \beta$, $d(0) = 0$ leaves the set S through ∂S_2. Proceeding as in [11, 12], one shows that the sets A and B are non-empty, open and ordered. Hence $\sup A =: \bar{\alpha} \leqslant \bar{\beta} := \inf B$, where $\bar{\alpha} \notin A$ and $\bar{\beta} \notin B$.

This means that for any $u_0 \in [\bar{\alpha}, \bar{\beta}]$ the half-orbit corresponding to Problem (P^+) ends in the point (u_s, d_*) as $\eta \to \infty$. This gives the required solution in terms of $u = u(\eta)$, $d = d(\eta)$ for $\eta > 0$. The solution for $\eta < 0$ is obtained by explicitly solving (P^-):

$$u(\eta) = (u_0 - u^*) \exp\left(\frac{q^* - a}{D}\eta\right) + u^*. \tag{4.9}$$

It is now easily checked that all the conditions in Definition 1 are satisfied. □

Theorem 4.6 *Suppose there exist two travelling-wave solutions, characterized by* (u_1, d_1, w_1, q_1) *and* (u_2, d_2, w_2, q_2), *for the same boundary conditions from class I. Then there exists* $\eta_0 \in \mathbb{R}$ *such that*

$$(u_1(\cdot), d_1(\cdot), w_1(\cdot), q_1(\cdot)) = (u_2(\cdot + \eta_0), d_2(\cdot + \eta_0), w_2(\cdot + \eta_0), q_2(\cdot + \eta_0)).$$

Proof Given both travelling waves, we apply to each a shift such that

$$d_1(\eta),\ d_2(\eta) > 0, \quad \text{for} \quad \eta > 0,$$
$$d_1(\eta) = d_2(\eta) = 0, \quad \text{for} \quad \eta \leqslant 0.$$

Then

$$w_1(\eta) = w_2(\eta) = 1, \quad \text{for} \quad \eta > 0.$$

We assume, without loss of generality, that $u_1(0) > u_2(0)$. Suppose that $u_1(\eta) \leqslant u_2(\eta)$ for $\eta > 0$, then

$$\lim_{\eta\to\infty} d_1(\eta) = \lim_{\eta\to\infty} \int_0^\eta \frac{k}{a\rho}(1 - r(u_1(\theta))\, d\theta < \lim_{\eta\to\infty} \int_0^\eta \frac{k}{a\rho}(1 - r(u_2)(\theta)\, d\theta = \lim_{\eta\to\infty} d_2(\eta),$$

which contradicts the boundary conditions for $\eta \to \infty$. This means that there exists an $\eta^* \in \mathbb{R}$, with $\eta^* > 0$, such that $u_1(\eta^*) < u_2(\eta^*)$, and by the continuous differentiability of

https://doi.org/10.1017/S0956792508007651 Published online by Cambridge University Press

u_1 and u_2, there exists an $\eta_* \in \mathbb{R}$, with $\eta_* > 0$, such that

$$u_1(\eta_*) = u_2(\eta_*), \tag{4.10}$$

$$u_1(\eta) \geqslant u_2(\eta), \quad \text{for} \quad \eta \in [0, \eta_*], \tag{4.11}$$

$$u_1'(\eta_*) \leqslant u_2'(\eta_*). \tag{4.12}$$

By (4.11), $d_1(\eta_*) < d_2(\eta_*)$. We compute, using (4.7) and (4.10),

$$u_1'(\eta_*) - u_2'(\eta_*) = 2\frac{[(q^* - a)(u_1(\eta_*) - u^*) - a(\rho - Mu_1(\eta_*))](d_1(\eta_*) - d_2(\eta_*))}{(1 - 2d_1(\eta_*))(1 - 2d_2(\eta_*))D}, \tag{4.13}$$

where $M = 1 - K$. It is now our aim to derive a contradiction to (4.12), so let us focus on the sign of

$$(q^* - a)(u_1(\eta_*) - u^*) - a(\rho - Mu_1(\eta_*)).$$

Using the expression (4.5) for the wave speed a, we obtain

$$\begin{aligned}(q^* - a)&(u_1(\eta_*) - u^*) - a(\rho - Mu_1(\eta_*)) \\ &= q^* \frac{-(u_s - u^*)(\rho + Ku_1(\eta_*) - u^*) + (u_1(\eta_*) - u^*)[2d_*(\rho - u_sM) + u_s - u^*]}{2d_*(\rho - u_s(1 - K)) + u_s - u^*}.\end{aligned}$$

Now, using $d_* < 1/2$, $u^* < u_s$, $u < u_s$ and the bounds (2.14) on K, we estimate

$$\begin{aligned}(q^* - a)&(u_1(\eta_*) - u^*) - a(\rho - Mu_1(\eta_*)) \\ &< q^* \frac{-(u_s - u^*)(\rho + Ku_1(\eta_*) - u^*) + (u_1(\eta_*) - u^*)[(\rho - u_sM) + u_s - u^*]}{2d_*(\rho - u_sM) + u_s - u^*} \\ &= \frac{q^*(u_1(\eta_*) - u_s)(\rho - Mu^*)}{2d_*(\rho - u_sM) + u_s - u^*} < 0.\end{aligned}$$

Together with (4.13), this gives $u_1'(\eta_*) - u_2'(\eta_*) > 0$, which contradicts (4.12). This means that our original assumption that $u_1(0) > u_2(0)$ (and thus also the assumption $u_1(0) < u_2(0)$) does not hold, so we have $u_1(0) = u_2(0)$, which implies that $u_1 = u_2$, $d_1 = d_2$, $w_1 = w_2$ and $q_1 = q_2$ on $\mathbb{R}$. □

5 Fixed versus variable geometry

In this section we compare the variable geometry situation as studied in the previous sections with the fixed geometry situation as studied in [14] and [12].

5.1 Fixed geometry as the limit $\rho \to \infty$

If we introduce the unknown $v^\epsilon := \rho d^\epsilon$, substitute this into the equations (2.9)–(2.12) and let $\rho \to \infty$, we obtain formally

$$\begin{cases} u_t^\epsilon = \nabla \cdot (D\nabla u^\epsilon - q^\epsilon u^\epsilon), \\ \epsilon^2 \mu \Delta q^\epsilon = \nabla p^\epsilon, \\ \nabla \cdot q^\epsilon = 0, \\ u^\epsilon,\ q^\epsilon,\ \text{and}\ p^\epsilon\ \text{symmetric around}\ y = 0, \end{cases} \qquad \text{in } \Omega^\epsilon(0) \tag{5.1}$$

https://doi.org/10.1017/S0956792508007651 Published online by Cambridge University Press

$$\begin{cases} d_t^\epsilon = 0, \\ v_t^\epsilon = k(r(u) - w), \\ w \in H(v^\epsilon), \qquad \text{on } \Gamma^\epsilon(0) \\ Dv^\epsilon \cdot \nabla u^\epsilon = -\epsilon v_t^\epsilon, \\ q^\epsilon = 0, \end{cases} \tag{5.2}$$

$$\begin{cases} u^\epsilon = u_b, \quad q^\epsilon = q_{bi}, \quad \text{on } \Gamma_i(0) \\ u_x^\epsilon = 0, \quad q^\epsilon = q_{bo}, \quad \text{on } \Gamma_o(0) \end{cases} \tag{5.3}$$

$$\begin{cases} u^\epsilon(x, y, 0) = u_I(x, y), \\ v^\epsilon(x, 0) = v_I(x). \end{cases} \tag{5.4}$$

These are the same equations as the equations studied in [14] (with a slightly different scaling of v^ϵ). In [14, Theorem 4.7] it is proven rigorously that for the limit $\epsilon \to 0$ solutions of (5.1)–(5.4) converge to solutions of the equations

$$\begin{cases} \partial_t(u_0 + 2v_0) = \partial_x(D\partial_x u_0 - \bar{q}u_0), \\ \partial_x \bar{q} = 0, \\ \partial_t v_0 \in k(r(u_0) - H(v_0)). \end{cases} \tag{5.5}$$

We can also obtain the equations (5.5) formally from the equations (3.10) by substituting $v_0 = \rho d_0$ and sending $\rho \to \infty$.

5.2 Comparison of wave speeds

In this section we compare the travelling-wave solutions of the fixed geometry case as studied in [12] and the travelling-wave solutions of the variable geometry case as studied in the previous sections. In particular, we are interested in comparing the wave speeds for both situations. In order to do so, we introduce again the variable $v = \rho d$ and substitute this in (4.1):

$$\begin{cases} \partial_t((1 - 2v/\rho)u + 2v) - \nabla \cdot ((1 - 2v/\rho)\nabla u - qu) = 0, \\ \partial_t v \in k(r(u) - H(d)), \\ \partial_x q - 2K\partial_t v/\rho = 0. \end{cases} \tag{5.6}$$

We impose the following boundary conditions from class I, so that a dissolution wave exists

$$\begin{cases} v(-\infty) = 0, & v(\infty) = v_* \\ u(-\infty) = u_* < u_s, & u(\infty) = u_s, \end{cases}$$

with $v_* < \rho/2$. Now we would like to compare the situation for a given, fixed value of ρ with the situation $\rho = \infty$, which corresponds to the equations (5.5) for the fixed geometry

https://doi.org/10.1017/S0956792508007651 Published online by Cambridge University Press

case. To this end, we introduce the parameter α in the equations in the following way:

$$\begin{cases} \partial_t((1-2\alpha v/\rho)u+2v)-\nabla\cdot((1-2\alpha v/\rho)\nabla u-qu)=0, \\ \partial_t v \in k(r(u)-H(d)), \\ \partial_x q-2\alpha K\partial_t v/\rho=0. \end{cases} \tag{5.7}$$

For $\alpha = 1$, we are in the case we have discussed in Section 4, and for $\alpha = 0$ we are in the case as discussed in [12]. It can be checked that all the results presented in the previous section also hold true for all $\alpha \in [0,1]$. This means that there exists, for boundary conditions from class I, a unique travelling-wave solution to the system of equations (5.7). The wave speed is then given by

$$a(\alpha) = \frac{u_s - u^*}{2v_*(1-\alpha u_s(1-K)/\rho)+u_s-u^*}q^*. \tag{5.8}$$

We prove the following proposition.

Proposition 5.1 *For $1-\rho/u_s < K < 1$ and $0 \leqslant \alpha \leqslant 1$, $a(\alpha)$ is increasing in α.*

Proof Computing the derivative in (5.8) with respect to α, we obtain

$$a'(\alpha) = \frac{u_s-u^*}{(2v_*(1-\alpha u_s(1-K)/\rho)+u_s-u^*)^2}2v_*u_s(1-K)q^*/\rho.$$

Since for the denominator we have, using the bounds (2.14),

$$2v_*(1-\alpha u_s(1-K)/\rho)+u_s-u^* \geqslant 2v_*(1-u_s(1-K)/\rho)+u_s-u^* \geqslant u_s-u^* > 0,$$

the proof is complete. □

From the lemma above, we can deduce that dissolution fronts will travel faster in the variable geometry case. This is also confirmed in the numerical experiments in Section 6. Note, however, that we compare the two situations where the inflow velocity is given. This means that in the variable geometry case the pressure drop is larger since part of the flow channel is narrower.

We may also compare the two situations with a given average pressure gradient. The pressure gradient is given by (cf. (3.8))

$$\partial_x p = -\frac{3q}{2(1/2-\alpha v/\rho)^3},$$

and we define the average pressure gradient P as follows

$$P := \lim_{\eta\to\infty}\frac{p(\eta)-p(-\eta)}{2\eta}.$$

https://doi.org/10.1017/S0956792508007651 Published online by Cambridge University Press

For the fixed geometry case, i.e. for $\alpha = 0$, we have $\partial_x p = 12q$ so that

$$\frac{p(\eta) - p(-\eta)}{2\eta} = \frac{1}{2\eta}\int_{-\eta}^{\eta} \partial_x p(x)\,dx = -\frac{24\eta\mu q}{2\eta} = -12\mu q^*,$$

and we have $P_{\text{fix}} = -12\mu q^*$. For the variable geometry case, i.e. for $\alpha = 1$, we have

$$\int_{-\eta}^{\eta} \partial_x p(x)\,dx = \int_{-\eta}^{\eta} \frac{-3\mu\bar{q}}{2(1/2 - v/\rho)^3}\,dx = \int_{-\eta}^{\eta} \frac{-3\mu(q^* - 2aKv/\rho)}{2(1/2 - v/\rho)^3}\,dx,$$

where we have used (4.3). It can be shown that

$$P_{\text{var}} = \frac{1}{2}q^*\left(-12\mu - \frac{3\mu(1 - 2\bar{a}Kv_*/\rho)}{2(1/2 - v_*/\rho)^3}\right),$$

where $\bar{a} = a/q^*$. By the previous result, for a given q^*, $P_{\text{var}} < P_{\text{fix}}$. Now, however, we fix $P_{\text{var}} = P_{\text{fix}} = P$ simultaneously for both situations, and solve for q^*_{fix} and q^*_{var}:

$$q^*_{\text{fix}} = -\frac{P}{12\mu},$$

and

$$q^*_{\text{var}} = P\left(-6\mu - \frac{3\mu(1 - 2\bar{a}Kv_*/\rho)}{4(1/2 - v_*/\rho)^3}\right)^{-1}.$$

For the corresponding wave speeds, we obtain

$$a_{\text{fix}} = -\frac{P}{12\mu}\frac{u_s - u^*}{2v_* + u_s - u^*}$$

and

$$a_{\text{var}} = P\left(-6\mu - \frac{3\mu(1 - 2\bar{a}Kv_*/\rho)}{4(1/2 - v_*/\rho)^3}\right)^{-1}\frac{u_s - u^*}{2v_*(1 - u_s(1 - K)/\rho) + u_s - u^*}.$$

In order to determine for which boundary conditions $a_{\text{fix}} > a_{\text{var}}$ and vice versa, we equate the two wave speeds and solve for u^* in terms of v_*:

$$u^* = u_s + \frac{2(v_*/\rho)u_s(1 - K)(1 + (1 - 2v_*/\rho)^3) + 2v_*((1 - 2v_*/\rho)^3 - 1)}{(1 - 2v_*/\rho)^3 - (1 - 2Kv_*/\rho)} =: g(v^*).$$

Define the set

$$X := \{(v_*, u^*) \mid 0 \leqslant u^* < \min(u_s, g(v_*)),\ 0 < v_* < \rho/2\}.$$

Then we have that $a_{\text{fix}} > a_{\text{var}}$ if $(v_*, u^*) \in X$, $a_{\text{fix}} = a_{\text{var}}$ if $u^* = g(v_*)$ and $a_{\text{fix}} < a_{\text{var}}$ otherwise.

https://doi.org/10.1017/S0956792508007651 Published online by Cambridge University Press

6 Numerical experiments

In this section we present the results of some numerical experiments and compare these results with the results obtained in the previous sections. First we will briefly discuss the numerical methods used for the computations.

6.1 Arbitrary Lagrangian–Eulerian method

For the computation for the microscale model equations we use the arbitrary Lagrangian–Eulerian (ALE) method [2]. This method has been developed to solve partial differential equations on moving domains. In this method the partial time derivatives are expressed with respect to a fixed reference configuration. A map, called the ALE map, $\chi_t : \Omega_0 \to \Omega(t)$, associates, at each time t, a point in the current computational domain $\Omega(t)$ with a point in the reference domain Ω_0. In this way, the system of ordinary differential equations resulting after space discretization describes the evolution of the solutions along trajectories that are at all times contained in the computational domain. We use the ALE method as implemented in the COMSOL Multiphysics package (http://www.comsol.com.) with Laplacian smoothing [2].

6.2 Numerical results

In this section we compare the numerical solution of the systems (2.9)–(2.12) with those of the system (5.7) for $\alpha = 0$ and $\alpha = 1$. We solve the system (5.7) on the interval $[0, 1]$ with boundary conditions

$$u(0,t) = 0, \quad u_x(1,t) = 0 \text{ and } \quad q(0,t) = 1/3 \cdot 10^{-1},$$

and initial conditions

$$v(x,0) \equiv 0.5 \quad \text{and} \quad u(x,0) \equiv 1 = u_s.$$

The parameter values used for the numerical experiments are

$$D = 10^{-3}, \ \ \rho = 2, \ \ k = 0.2, \ \ r(u) = u, \ \ K = 0.1.$$

These parameter values do not necessarily correspond to a realistic situation. The main purpose of this section is to investigate how well the solution of the system (5.7) approximates the averaged solutions of (2.9)–(2.12). In particular, we chose the simplest rate function $r(u)$ that satisfies the assumptions given in Section 2. Also note that from the analysis in Section 4 it follows that the rate function does not influence the wave speed (as long as the value u_s does not change), it will only influence the shape of the front. We refer to [7] for a comparison of linear and non-linear rate functions.

For the systems (2.9)–(2.12) we use for the boundary and initial conditions

$$u_b \equiv 0, \ \ v_I(x) \equiv 0.5 \quad \text{and} \quad u_I(x,y) \equiv 1 = u_s.$$

The inflow velocity for the systems (2.9)–(2.12), i.e. q^ϵ at $x = 0$, is given by a parabolic velocity profile such that the average velocity matches $q(0,t)$ as given above. At $x = 1$ we impose $p^\epsilon I + \frac{\mu}{2}(\nabla q^\epsilon + (\nabla q^\epsilon)^T) = 0$.

https://doi.org/10.1017/S0956792508007651 Published online by Cambridge University Press



FIGURE 2. Profiles of the concentration u^ϵ with $\epsilon = 0.1$ for the 2-D model for $t = 0$, $t = 10$, $t = 20$, $t = 30$ and $t = 40$, respectively. The dark regions at the left indicate low concentrations, the dark regions at the right indicate high concentrations and the lighter regions in the middle indicate the transition between low and high concentrations. Also the changes in the width of the strip are depicted.

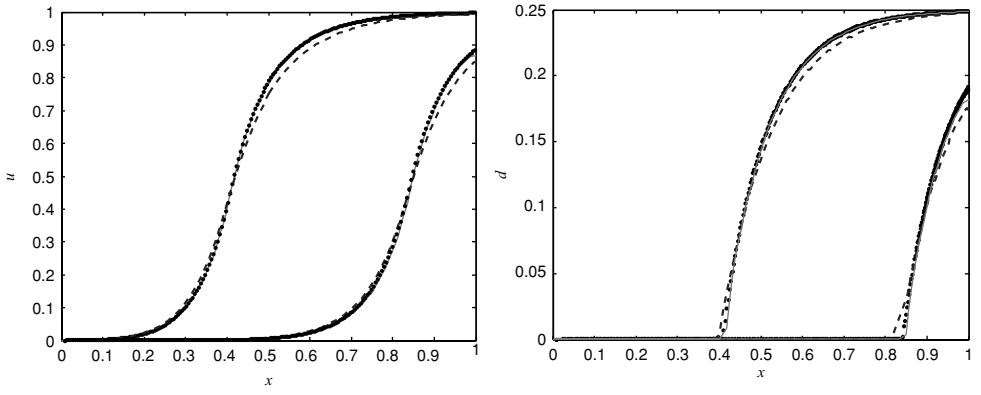


FIGURE 3. Profiles of both the two-dimensional and effective models for $t = 20$ and $t = 40$. The left plot shows profiles for u and u^ϵ, the right plot shows d and d^ϵ. The solid line represents the solution to the effective model, the dashed line the two-dimensional model with $\epsilon = 0.1$ and the dots represent the two-dimensional model with $\epsilon = 0.01$.

With the parameter values given above we can compute an approximation of the speed of the dissolution front, using (4.5) for the speed of a travelling wave:

$$a_{\text{fix}} = \frac{1}{2}q^* = \frac{1}{60} \approx 0.01667,$$
$$a_{\text{var}} = \frac{20}{31}q^* = \frac{20}{930} \approx 0.02151.$$

In Figure 2, the concentration profiles of u^ϵ, solving the equations (2.9)–(2.12), are plotted for different values of t. Also the changes in the width of the strip are depicted. These profiles are compared to profiles obtained by solving the effective model equations (5.7) for $\alpha = 1$ (Figure 3). In the left plot the profiles of $u^\epsilon(x, 0, t)$ for two different values of

https://doi.org/10.1017/S0956792508007651 Published online by Cambridge University Press

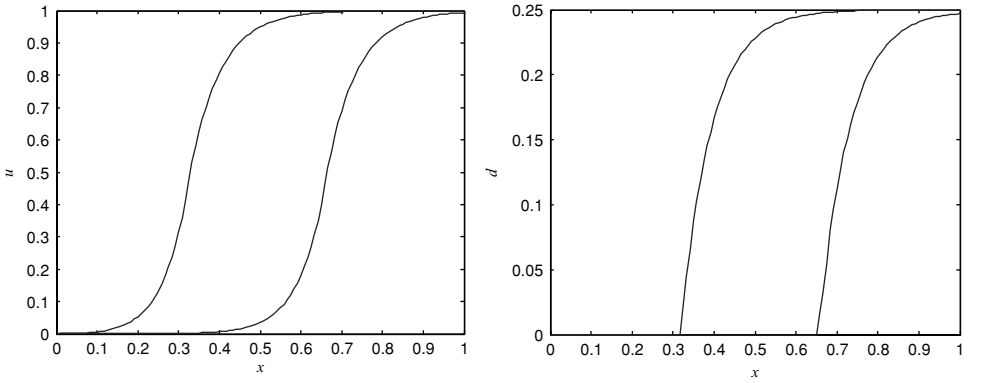


FIGURE 4. Profiles of solutions to the effective model for the fixed geometry case, for $t = 20$ and $t = 40$. The left plot shows profiles for u, the right plot shows d.

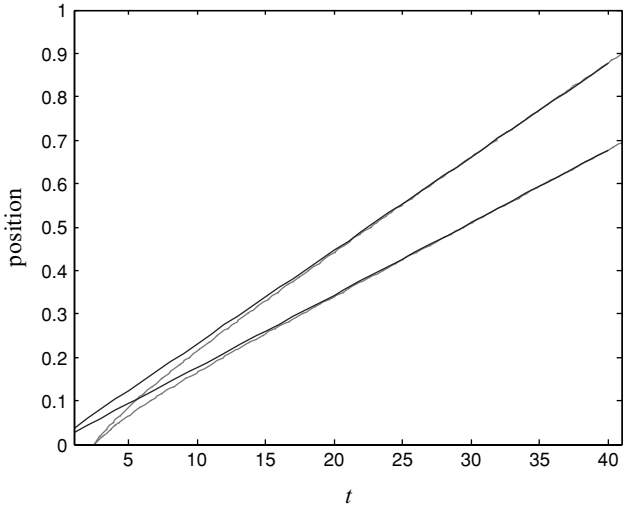


FIGURE 5. The position of the free boundary versus time for both the fixed and variable geometry effective models. Two lines with slopes $a_{\text{fix}} = 1/60 \approx 0.01667$ and $a_{\text{var}} = 20/930 \approx 0.02151$ are also plotted to indicate the wave speed as predicted in (4.5).

ϵ are compared to the profiles of u solving (4.1). In the right plot the d^ϵ is compared to $d = v/\rho$. The profiles are plotted for the two values $t = 20$ and $t = 40$. The thin continuous lines correspond to u and d, the dashed line corresponds to u^ϵ and d^ϵ for $\epsilon = 0.1$ and the dots correspond to u^ϵ and d^ϵ for $\epsilon = 0.01$. We see that for both values of ϵ the effective model describes the behaviour of solutions of the microscale model quite well, and for $\epsilon = 0.01$ the differences are even hardly distinguishable.

Figure 4 shows the profiles of u and $d = v/\rho$ that solve the equations (5.7) corresponding to the fixed geometry case, i.e. for $\alpha = 0$. We see clearly that the front did not move as fast to the right as for the variable geometry case.

In Figure 5, the speed of the dissolution front is showed in more detail. The position of the free boundary of the thickness of the crystalline solid is compared with the wave speed

https://doi.org/10.1017/S0956792508007651 Published online by Cambridge University Press

as predicted in (4.5), both for the variable and the fixed geometry case. We see that after a start-up phase the speed of the free boundaries match very well with the predicted values.

7 Conclusions

In this paper we have derived a macroscopic model for crystal dissolution and precipitation in porous media. The model takes into account the change in porosity and permeability due to the change in the local pore geometry. The macroscopic model was derived using a formal limiting argument and the behaviour of solutions was validated using numerical experiments.

Also travelling-wave solutions of the macroscopic model were studied and compared to travelling-wave solutions of previously published models [12, 14]. Just as for the model in [12], only dissolution waves exist. The wave speed for a fixed inflow velocity is faster for the model equations presented in this paper.

Acknowledgements

The author wishes to thank I. S. Pop, C. J. van Duijn and M. A. Peletier for the discussions that helped to shape this work. Part of this research has been funded by the Dutch BSIK/BRICKS project.

References

[1] Brown, R., Hu, W. & Lieberman, G. (1997) Weak solutions of parabolic equations in non-cylindrical domains. *Proc. Amer. Math. Soc.* **125**, 1785–1792.

[2] Donea, J., Huerta, A., Ponthot, J.-Ph. & Rodríguez-Ferran, A. (2004) Arbitrary Lagrangian–Eulerian methods. In: E. Stein, R. De Borst & T. J. R. Hughes (editors), *Encyclopedia of Computational Mechanics, Vol. 1(Fundamentals)*, Chap. 14, John Wiley & Sons.

[3] Eymard, R., Gallouët, T., Herbin, R., Hilhorst, D. & Mainguy, M. (1999) Instantaneous and non-instantaneous dissolution: Approximation by the finite volume method. In: *Actes du 30ème Congrès d'Analyse Numérique: CANum '98 (Arles, 1998)*, vol. 6 of *ESAIM Proc.*, pp. 41–55 (electronic). Soc. Math. Appl. Indust., Paris.

[4] Fasano, A. (2005) Mathematical models of some diffusive processes with free boundaries, vol. 11 of *MAT. Serie A: Conferencias, Seminarios y Trabajos de Matemática [MAT. Series A: Mathematical Conferences, Seminars and Papers]*. Universidad Austral, Facultad de Ciencias Empresariales (FCE-UA), Departamento de Matemática, Rosario.

[5] Faugeras, B., Pousin, J. & Fontvieille, F. (2006) An efficient numerical scheme for precise time integration of a diffusion-dissolution/precipitation chemical system. *Math. Comp.* **75**(253), 209–222 (electronic).

[6] Hornung, U., Jäger, W. & Mikelić, A. (1994) Reactive transport through an array of cells with semi-permeable membranes. *RAIRO Modél. Math. Anal. Numér.* **28**(1), 59–94.

[7] Knabner, P., van Duijn, C. J. & Hengst, S. (1995) An analysis of crystal dissolution fronts in flows through porous media. Part 1: Compatible boundary conditions. *Adv. Water Res.* **18**, 171–185.

[8] Maisse, E. & Pousin, J. (1997) Diffusion and dissolution/precipitation in an open porous reactive medium. *J. Comput. Appl. Math.* **82**(1–2), 279–290. 7th ICCAM 96 Congress (Leuven).

https://doi.org/10.1017/S0956792508007651 Published online by Cambridge University Press

[9] Tartakovsky, A. M., Scheibe, T., Redden, G., Meakin, P. & Fang, Y. (2006) Smoothed particle hydrodynamics model for reactive transport and mineral precipitation. In: P. J. Binning, P. K. Engesgaard, H. K. Dahle, G. F. Pinder & W. G. Gray (editors), *Proceedings of the XVI International Conference on Computational Methods in Water Resources*, June 2006, Copenhagen, Denmark. http://proceedings.cmwr-xvi.org.

[10] Tartakovsky, A. M., Meakin, P., Scheibe, T. D. & Eichler West, R. M. (2007) Simulations of reactive transport and precipitation with smoothed particle hydrodynamics. *J. Comput. Phys.* **222**(2), 654–672.

[11] van Duijn, C. J. & Knabner, P. (1991) Solute transport in porous media with equilibrium and non-equilibrium multiple-site adsorption: Travelling waves. *J. Reine Angew. Math.* **415**, 1–49.

[12] van Duijn, C. J. & Knabner, P. (1997) Travelling wave behaviour of crystal dissolution in porous media flow. *European J. Appl. Math.* **8**(1), 49–72.

[13] van Duijn, C. J., Peletier, L. A. & Schotting, R. J. (1993) On the analysis of brine transport in porous media. *European J. Appl. Math.* **4**(3), 271–302.

[14] van Duijn, C. J. & Pop, I. S. (2004) Crystal dissolution and precipitation in porous media: Pore scale analysis. *J. Reine Angew. Math.* **577**, 171–211.

[15] van Duijn, C. J. & Schotting, R. J. (1998) Brine transport in porous media: On the use of Von Mises and similarity transformations. *Comput. Geosci.* **2**(2), 125–149.

[16] van Noorden, T. L. & Pop, I. S. (2008) A Stefan problem modelling dissolution and precipitation. *IMA J. Appl. Math.* **73**, 393–411.

[17] van Noorden, T. L., Pop, I. S. & Röger, M. (2007) Crystal dissolution and precipitation in porous media: L^1-contraction and uniqueness. *Discrete Contin. Dyn. Syst.*, suppl., 1013–1020.

https://doi.org/10.1017/S0956792508007651 Published online by Cambridge University Press